15TH IEA HEAT PUMP CONFERENCE
MAY 26–29, 2026 | HOFBURG
VIENNA 2026
DECARBONISATION THROUGH INNOVATION

Experimental investigation of a heat pump coupled to a thermal storage for charging a Carnot battery

Simon Schmeing[a,*], Alexandra Welp[a], Burak Atakan[a]

[a]University of Duisburg-Essen, Thermodynamics, EMPI, 47057 Duisburg, Germany

Abstract

Carnot batteries (CBs) are commonly charged using heat pumps, yet experimental data for model validation remain limited. We designed and commissioned a flexible, highly instrumented, laboratory-scale test bench and report initial CB charging experiments. The setup uses a 3.3 kW reciprocating compressor in the heat pump and incorporates two unpressurized water storage tanks for energy storage; the condenser heats water transferred from one tank to the other. Two plate heat exchangers ensure deep subcooling below 25 °C, which reduces throttling losses and enables CB start-up from ambient temperature. Tap water entering at ambient temperature served as heat source, limiting the minimum temperature. We compare a zeotropic working fluid mixture (propane/pentane) with two pure fluids (propane and butane), focusing on irreversibilities in the condenser and compressor. We assess the impact of operating conditions on cycle and component efficiencies by varying the upper storage temperature from 45 °C to approximately 90 °C and exploring compressor outlet temperatures ranging from 70 to 118 °C. The process-dependent overall compressor efficiency of the mixture ranges from 47 to 57%, which exceeds the efficiency of pure butane. The mixture reduces exergy destruction rates during heat rejection to the sensible storage tanks compared to the pure fluids, but increases exergy destruction rates during evaporation against a near-isothermal heat source, the latter reduces the second-law efficiency. Finally, a reciprocating-compressor model is compared with the measurements, indicating its potential for heat pump simulation.

© HPC2026.
Selection and/or peer-review under the responsibility of the organizers of the 15th IEA Heat Pump Conference 2026.

Keywords: refrigerant mixture; zeotropic mixture; temperature glide; Carnot battery; high-temperature heat pump

1. Introduction

The increasing share of renewable electricity generation is predicted to result in increased energy storage needs, when large degrees of decarbonization are aimed for [1]. Carnot batteries (CBs) are an alternative site-independent electricity storage technology, which has received increased research attention in recent years. There exist various CB concepts, as summarized by Dumont et al. [2]. Typically, a high temperature heat pump is used for charging the thermal energy storage (TES) of the CB during periods of electricity surplus. Within the realm of CBs based on the Rankine cycle, commonly pure working fluids (WFs) are investigated [2]. In contrast, some concepts use a zeotropic working fluid mixture, typically in combination with a sensible TES. A major motivation is the improvement of the temperature profile matching between the working fluid and sensible TES and thus reducing irreversibilities of heat transfer [3] and ultimately increasing the round-trip efficiency. Mostly theoretical CB concepts using working fluid mixtures have been discussed in the literature so far, for example:

Koen et al. [3] optimized the composition of a quaternary WF mixture based on linear alkanes, resulting in a near constant effective heat capacity in the two-phase region (i.e., a "linear" temperature glide) and an

* Corresponding author. Tel.: +49-203-3793233
E-mail address: simon.schmeing@uni-due.de

improved temperature profile matching. The heat pump (HP) operated at temperatures between 0 and 100 °C, with a WF temperature glide of ca. 35 °C and temperature changes in the storages of up to 47 °C, while the baseline pre-charge temperature of one storage was 58.8 °C. The calculations were carried out for three different fixed isentropic machine efficiencies. HP exergetic losses of 23.3% of the input power are reported.

Bernehed [4] simulated a CB with an ammonia-water mixture of varying composition. Eight parameters that affect the round-trip efficiency were varied to analyze their influence. Among them were assumed constant machine efficiencies and the upper process temperature, which was varied up to 450 °C. Some of the storages require initial temperatures of ca. 100 to 200 °C. The author found that machine efficiencies play an important role, but the largest entropy generation occurs due to temperature-profile mismatch in the heat exchangers.

Welp and Atakan [5] investigated a ternary hydrocarbon WF mixture in a parametric study. The influence of pressure ratio, temperature difference during heat transfer, and mixture composition on the round-trip efficiency was studied for storages, of which one is initially not at ambient temperature. Their work included a semi-empirical compressor model to include realistic compressor efficiencies, that covers the influence of operating conditions and mixture composition. Other machinery was modelled with constant isentropic efficiencies. Pressure ratios of 10 to 11 were found optimal for high round-trip efficiencies, resulting in compressor outlet temperatures up to ca. 400 K.

The reviewed CB concepts use different numbers and types of TES for the different sections of heat transfer, but at least one TES starts operation at a temperature different from ambient. The questions – how the TES are brought to the starting temperature, how often this is required, and the associated energy demand – remain unaddressed. Its assessment requires data about charging, stillstand and discharging times, but also necessitates experimental investigation. Storages which are initially at ambient temperature – as investigated here – simplify the system and reduce losses during initial start-up.

To date, only one experimental study on Carnot batteries using a WF mixture has been reported: Weitzer et al. [6] experimentally investigated a WF mixture of R-1336mzz(Z) and R-1336mzz(E) in a CB originally designed for pure WFs [7]. The mole fraction of R-l336mzz(Z) was varied from 0 to 1, resulting in a maximum temperature glide of 6.2 °C (at a dew point temperature of 30 °C). A sensible TES with relatively small temperature changes, between 5 and 30 °C, was used. Despite high TES temperatures up to 110 °C, the temperature lift (temperature difference between heat source and sink) is limited, as process heat at an inlet temperature of 80 °C is used as heat source. They found a relative improvement of the coefficient of performance (*COP*) of 11% for the best performing mixture (10 wt.-% R-l336mzz(E)) compared to the better performing pure fluid R-l336mzz(Z). This work is limited by the relatively small overall temperature lift and the low temperature glide of the tested working fluids. For CB applications, mixtures with a higher temperature glide are promising [3–5]. Larger glides are beneficial for utilizing sensible TES with high energy density, requiring large temperature changes in the storage, while maintaining a good temperature matching between storage and WF. Furthermore, round-trip efficiencies increase with the temperature lift [8,9].

For pure charging and discharging cycles, more data can be found. But for heat pumps with WF mixtures, again experimental investigations are mostly limited to temperature glides below 15 °C, as reviewed by Brendel et al. [10]. Many experimental investigations are available for residential heat pumps (e.g. [11,12]), operating at lower temperatures than required for CB applications. The conditions for industrial heat pumps are more relevant for CBs. For such, Brendel et al. conducted an experimental study focusing on binary and ternary HFO and HCFO mixtures [10] with temperature glides between 10 and 40 °C and varying composition. They systematically varied the temperature changes in the heat sink and source, with values up to 35 °C. Temperature levels were also varied, with heat sink inlet-temperatures between 80 and 120 °C resulting in temperature lifts of up to 80 °C. The authors found improvements in the *COP* of 16% for the best mixture compared to the best pure WF. Further, the mixtures show a more robust *COP* against changed temperature levels. In a similar study, Brendel et al. [13] investigated the hydrocarbon mixtures propane/butane and propane/pentane at various mole fractions. Heat source inlet and sink outlet temperatures were kept at 60 °C and 100 °C, respectively. The temperature change of both the heat sink and the source were controlled to be 35 °C. They found propane/pentane at a molar composition of 70/30% to be the mixture with the highest *COP* of 3.16. Compared to the best-performing pure fluid, butane, the *COP* was 19% higher.

Despite these efforts, experimental data for heat pumps using large temperature glide WF mixtures at high sink temperatures around 90 °C are scarce. Addressing this research gap, this study presents a novel experimental set-up of the charging HP of a Carnot battery running on WF mixtures. The final concept, is to have a fully functional Carnot battery with up to four storages, three at high temperature and one at low temperature, to have a good temperature matching. Here, only the charging cycle with one high-temperature storage was set up and analyzed, concentrating on the exergy destruction in the heat rejection, the compressor, and the throttle as a function of working fluid and storage temperature. This will be extended in future. This work investigates a mixture with a high temperature glide, propane (R-290) and n-pentane (R-601), at elevated temperatures. The heat pump is coupled to a sensible thermal energy storage initially at ambient temperature, enabling start-up from ambient conditions and providing a more realistic operation than assuming arbitrarily high initial temperatures. We varied the maximum storage temperature up to 90 °C, resulting in storage-temperature changes of up to 70 °C. The reviewed literature, as well as further CB studies [14], show that compressor efficiency is often assumed to be constant. This assumption is examined by comparing the experimental data to a semi-empirical compressor model.

2. Methods

2.1. Experimental set-up

The experimental set-up consists of a laboratory-scale vapor-compression heat pump, which is coupled to a sensible two-tank TES. The HP is designed to operate with different hydrocarbon working fluid mixtures. The nominal compressor power is 3.3 kW_{el}. Temperature limits are 140 °C for the compressor outlet temperature and currently 100 °C for the TES, respectively. The working fluid pressure must be kept between 1 and 25 bar-a. The lower limit is a safety measure to prevent air intrusion, as flammable working fluids are used.

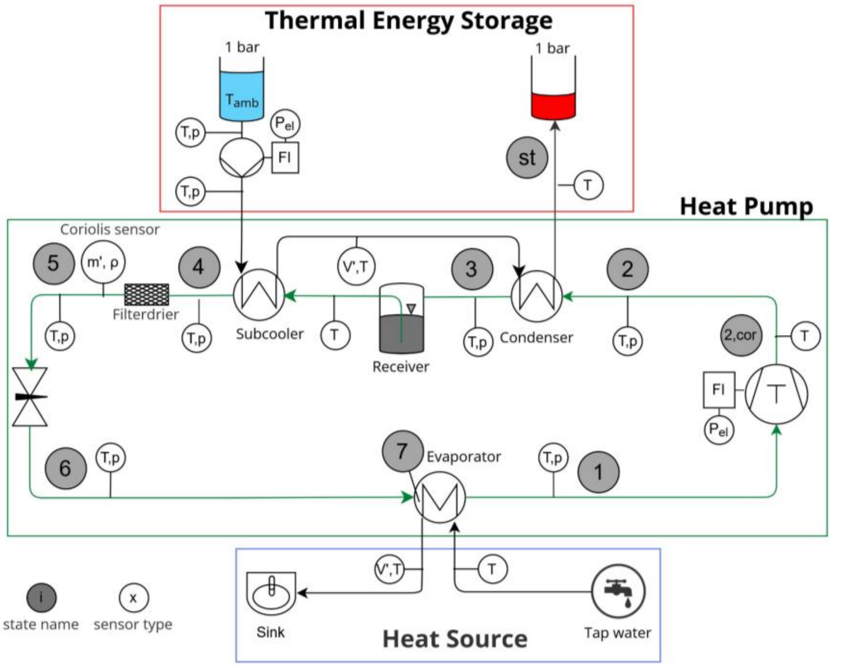

Fig. 1: Simplified process flow diagram of the experimental set-up.

A process flow diagram is shown in Fig. 1 and detailed information about the main components is provided in Table 1. The frequency of the reciprocating compressor can be adjusted by a frequency inverter (FI). The compressor is lubricated with a PAG oil and relies solely on its internal oil separator. For throttling, an electronic expansion valve is installed. Counterflow plate heat exchangers are used, with a distribution system [15] at the inlet port, for distributing a two-phase inlet-flow correctly on all plates, which can cause a significant pressure drop. The heat rejection to the TES is divided between two heat exchangers, referred to as the condenser and the subcooler, which are separated by a liquid receiver. The receiver accommodates excess working fluid and is sized to remain partially filled during operation. The TES serves as heat sink for the HP. It is designed as a two-tank storage. At the beginning of an experiment the storage fluid at ambient temperature is inside the first tank. It is then pumped through the HP's subcooler and condenser in series, where it is heated up, and is then stored inside the other tank at elevated temperature. Demineralized water at ambient pressure is used as the hot storage/secondary fluid (SFH). Tap water is used as cold secondary fluid (SFC) and serves as heat source.

Detailed information about the used measurement sensors is provided in Table 2. Temperatures and pressures on the working-fluid side are measured at the inlet and outlet of each main HP component. For the secondary fluid circuits, temperatures are measured at the inlet and outlet of each main component. The WF mass flow rate is measured with a Coriolis flow meter, and the secondary-fluid volumetric flow rates are measured with electromagnetic flow meters. The compressor's electrical power consumption is measured via the frequency inverter.

Table 1: Technical specifications of main components.

Component	Specifications
Compressor	Type: Reciprocating compressor, semi-hermetic Manufacturer, model: Bitzer, ECOLINE 2EESP Nominal power: 3.3 kW_{el} Oil: BSG68K (PAG oil), 1.5 L, density 1003 kg/m^3 (at 15 °C) [16] Geometric data [17]: piston diameter d = 4.6 cm, stroke h = 3.93 cm, number cylinders n_{cyl} = 2, pole-pair number n_{pole} = 2, outer surface area A = 0.485 m^2, ratio of crankshaft radius and connecting rod length $L = 3.5$* *Standard value as in Heywood [18], compressor model not strongly sensitive [19]
Frequency inverter (compressor)	Bitzer Varipack FMY+6-4,Frequency range: 35 …70 Hz
Condenser	Plate heat exchanger, SWEP FI22ASHx44, Area: 1.32 m^2
Subcooler	Plate heat exchanger, SWEP B8LASHx8, Area: 0.152 m^2
Evaporator	Plate heat exchanger, FI22ASMx28, Area: 0.819 m^2
Liquid receiver	Frigomec, custom-made, volume: 2.8 L
Electric expansion valve	Sanhua LPF08-003
Storage Pump (SFH)	Manufacturer: AFT, type: rotary vane, nominal flow: 300 L/h

A common phenomenon for zeotropic WF mixtures is the occurrence of a composition shift, which is defined as the difference between WF composition circulating in the cycle and filled-in composition. The circulating composition was determined using an established inline method, utilizing the density measurement of the Coriolis mass flow meter $\rho_{measured}$ [20]. The mole fraction x_A was inferred by also calculating the mixture density with an equation of state (EOS) ρ_{EOS} (T,p,x_A) and minimizing the difference between ρ_{EOS} and $\rho_{measured}$. Further, oil can be flushed out of the compressor as oil separation is not perfect. A similar method from literature [21] is used for finding the oil circulation rate for pure working fluids. As a simplification, it is assumed that WF and oil form an ideal solution, which may lead to inaccuracies [21]. It is assumed that the oil circulation rate remains unchanged for mixtures.

Table 2. Type and accuracy of measurement equipment. Accuracies are provided by manufacturers.

Measurement quantity	Sensor type	Sensor accuracies
Temperature	Resistance thermometer, Pt1000-AA, Sensor Electric SWM-025	0.1 + 0.0017 | T[°C] |
Pressure	Piezoelectric transducer, ICS Schneider IMP 331	0.1% of range = 0.025 bar
Mass flow rate (WF)	Coriolis mass flow meter, Krohne Optimass 6400	< 0.2% of reading
Density (WF)	“	1 kg/m^3 absolute
Volume flow rate (SFH and SFC)	Electromagnetic flowmeter, Krohne AF-E 400	< 1% of reading
Electrical compressor power	FI internal measurement, Bitzer Varipack FMY+6-4	10 W absolute

2.2. Data processing

After steady-state operation is reached, sensor signals are recorded for 10 min and the arithmetic mean values are further used. Properties are evaluated using the EOS from REFPROP [22]. As oil circulation rates are found to be very small, their potential influence on the thermodynamic properties is neglected. The thermodynamic state is usually fixed using temperature and pressure values. For the subcooled secondary fluids, pressure is not measured, but rather estimated to be 2 bar for all states. The throttle is assumed to be isenthalpic ($h_5 = h_6$). Analogously the WF state after the evaporator's distribution system is found by assuming a further isenthalpic expansion to the evaporator outlet pressure p_1 ($h_7 = h_6$).

If the measured condenser outlet temperature is above the bubble point temperature at the measured outlet pressure, this is treated as measurement error and the condenser outlet state is set to be at the bubble point (vapor quality q = 0), as shown in Eq. (1). Otherwise, temperature and pressure measurements are used.

$$h_3 = h(p_3, q = 0), \text{ if } T_3 \geq T'(p_3) \tag{1}$$

The coefficient of performance *COP* is calculated using the compressor FI's power consumption $P_{\text{comp,el}}$ and heat flow absorbed by the storage fluid $\dot{Q}_{\text{SFH}}$.

$$COP = \frac{\dot{Q}_{\text{SFH}}}{P_{\text{comp,el}}} = \frac{\dot{V}_{\text{SFH}}\, \rho_{\text{SFH}}\, \left(h_{\text{SFH,out}} - h_{\text{SFH,in}}\right)}{P_{\text{comp,el}}} \tag{2}$$

For reference the second-law efficiency η_{2nd} compares the actual *COP* with the efficiency of a reversible process COP_{max} that operates between the thermodynamic mean temperatures of the secondary fluids $\bar{T}_{\text{i}}$:

$$COP_{\text{max}} = \frac{\bar{T}_{\text{SFH}}}{\bar{T}_{\text{SFH}} - \bar{T}_{\text{SFC}}}, \quad \text{with} \quad \bar{T}_{\text{i}} = \frac{T_{\text{i,out}} - T_{\text{i,in}}}{ln(T_{\text{i,out}}/T_{\text{i,in}})} \tag{3}$$

$$\eta_{\text{2nd}} = \frac{COP}{COP_{\text{max}}} \tag{4}$$

The exergy destruction rate $\dot{Ex}_{\text{d,i}}$ is evaluated for each component i:

$$\dot{Ex}_{\text{d,i}} = P_{\text{el}} + \sum_{\text{in}} \dot{m}_{\text{j}}\, ex_{\text{j}} - \sum_{\text{out}} \dot{m}_{\text{j}}\, ex_{\text{j}} \tag{5}$$

The specific exergy of fluid stream j ex_{j} is evaluated using its properties at dead state (index "0"), which is defined to be at 293.15 K and 1 bar:

$$ex_j = h_j - h_0 - T_0\left(s_j - s_0\right) \tag{6}$$

The compressor's isentropic $\eta_{\text{comp,is}}$, global $\eta_{\text{comp,global}}$ and volumetric efficiency $\eta_{\text{comp,vol}}$ are defined in Eq. (7) - (9) and calculated using its stroke volume V_{stroke} and rotational speed n_{comp}. Non-negligible heat losses caused a measurable temperature drop between the compressor outlet and close to the condenser inlet, where the sensor measures temperature T_2. An additional temperature sensor was subsequently installed directly at the compressor outlet for the experiments with butane as working fluid. For the remaining experiments, T_2 was corrected based on the offset measurements with butane, assuming that it is fluid-independent. The correction ranged from 5 to 7 K, the corrected values will be reported as $T_{2,\text{cor}}$.

$$\eta_{\text{comp,is}} = \frac{h_{2,\text{is}} - h_1}{h_2 - h_1} = \frac{h(p_2, s_1) - h_1(T_1, p_1)}{h_2(T_2, p_2) - h_1(T_1, p_1)} \tag{7}$$

$$\eta_{\text{comp,global}} = \frac{\dot{m}_{\text{WF}}(h_{2,\text{is}} - h_1)}{P_{\text{comp,el}}} \tag{8}$$

$$\eta_{\text{comp,vol}} = \frac{\dot{m}_{\text{WF}}}{\rho_1(T_1, p_1) V_{\text{stroke}} n_{\text{comp}}} \tag{9}$$

2.3. Parameter study

Two pure working fluids, propane (C_3) and n-butane (C_4), and one binary mixture were investigated. The mixture consisted of propane and n-pentane (C_3/C_5), with an initial molar composition of x_{C3} = 80% and

x_{C5} = 20%. For each fluid the following parameter variations were performed: three compressor frequencies between 30 and 70 Hz and several storage inlet temperatures T_{st} between 45 and 90 °C were investigated, as shown in Table 4. The measured mixture composition is also given there. The following boundary conditions were set and maintained as constant as possible for all experiments, with slight variation between the working fluids. Both secondary fluid inlet temperatures were kept at ambient temperature. The mass flow of SFC was set to the maximum possible value for each experiment. The desired compressor frequency was set at the beginning of an experiment. The process was brought to the target storage inlet temperature T_{st} by manually adjusting the SFH mass flow rate via the storage-pump frequency. Simultaneously, the throttle-valve opening was manually adjusted to achieve a prescribed superheat at the evaporator outlet, in order to protect the compressor. The measured values are shown in Table 3.

Table 3. Realized values corresponding to the prescribed experimental boundary conditions, specific for each working fluid.

Boundary condition	C_3	C_4	C_3/C_5
Superheating after evaporator [°C]	17.0 … 17.9	9.0 … 15.1	12.2 ... 13.1
$\dot{m}_{SFC}$ [kg/min]	7.8 … 10.16	7.9 … 10.1	9.6 ... 10.1
$T_{SFH,in}$ [°C]	20.1 … 27.2	15.4 … 23.4	19.2 ... 31.1
$T_{SFC,in}$ [°C]	17.8 … 18.8	14.2 … 20.8	17.7 ... 18.7

Table 4. Overview of experimentally varied parameters (T_{st} and f_{comp}) for the three working fluids (C_3, C_4 and C_3/C_5). Measured circulating molar composition for the mixture is given in parentheses. Color highlights the working fluid. [rep] marks the experiment for which a reproduction experiment was performed. [fitting] indicates the experiment used for compressor model fitting.

Storage inlet temperature T_{st}	Compressor frequency f_{comp}			
	30 Hz	40 Hz	50 Hz	70 Hz
45 °C	C_3	-	-	-
55 °C	C_3	-	-	-
60 °C	-	C_4	C_4	C_3/C_5 (82.1/17.9%), C_4 [fitting]
65 °C	C_3	-	C_3	-
70 °C	C_3/C_5 (82.7./17.3%)	-	C_3/C_5 (82.5/17.5%)	C_3/C_5 (81.7/18.3%)
75 °C	-	-	-	C_4
80 °C	-	-	-	C_3/C_5 (81.9/18.1%)
90 °C	-	-	-	C_3/C_5 (81.3/18.7%) [rep], C_4

2.4. Experimental data quality

The uncertainties of the derived quantities are estimated using a Monte Carlo analysis employing the python package SALib [23]. The sum of sensor accuracies and the signal standard deviations during the 10-minute recording interval are used as the uncertainties of the measured quantities. A normal distribution is assumed for all signals. The calculated uncertainty of derived quantities is shown in the form of error bars in selected diagrams. The error bars indicate mean ± 2 standard deviations (approximate 95% coverage of individual observations). Further, one experiment was reproduced with more than 10 days between both experiments, as indicated with [rep] in Table 4. The *COP* changed from 2.13 to 2.10, a deviation of < 1.4%. The circulating mole fraction of C_3 was found to be x_3 = 81.3% and 81.5%, a deviation of < 0.25%. All oil content measurements found oil circulation rates below 0.2%; all but one being significantly lower. Thus, neglecting the effects of oil on WF properties seems justified.

2.5. Compressor model

We used the measurement results to evaluate a widely used reciprocating compressor model by comparing its predictions with the measurements. Prior studies show that isentropic efficiency and volumetric efficiency can vary substantially with the working fluid and operating conditions. Roskosch et al. [19] developed a semi-empirical model for reciprocating compressors, that was already tested for zeotropic mixtures and has to be calibrated at a single operating point per compressor. It iteratively solves the cycle considering internal compression work, mass transfer through the valves, friction losses and heat loss to the environment. Further details are given in the original publication [19].

The model does not include frequency variation effects. The calibration point was measured at 70 Hz, and only results at this frequency are discussed in the comparison. Geometric compressor data are provided in Table 1. For fitting, the 60 °C storage inlet temperature measurement point for butane is used (marked with [fitting] in Table 4) and results in a relative clearance volume of $c_{\mathrm{cl}} = 1.26\%$ and a friction pressure of $p_{\mathrm{fr}} = 5.4$ kPa. Both fitted parameters are then used to predict the mixture efficiencies.

3. Results and Discussion

In the following, first selected conditions are compared for pure fluids and fluid mixtures with respect to the losses in the condenser and other parts, before the compressor efficiencies are presented for different operating conditions and compared with the compressor model. Finally, the overall performance of the heat pump is discussed in terms of *COP*s and second-law efficiencies.

3.1. Heat exchanger temperature profile matching and exergy destruction

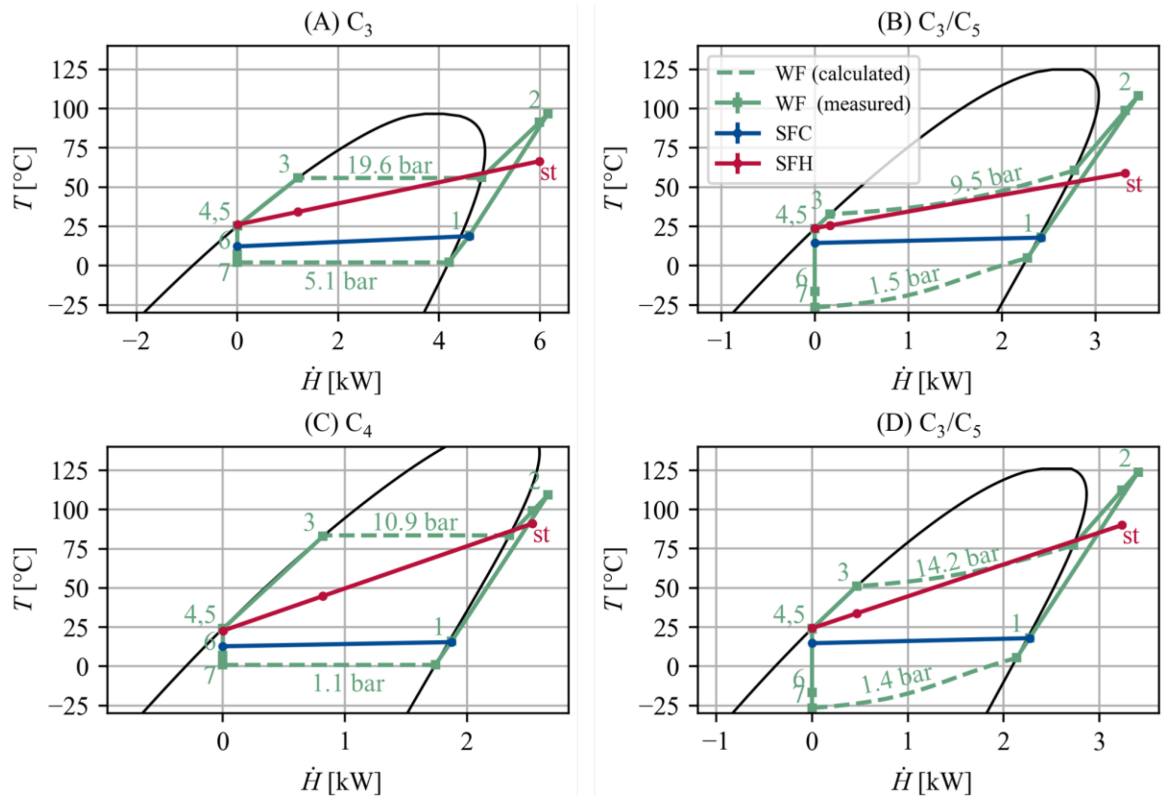

Fig. 2. Exemplary temperature-enthalpy flow (T-$\dot{H}$) diagrams of all working fluids at selected operating conditions. Error bars are shown for temperatures, but are barely visible at this scale. (A): working fluid C_3 at T_{st} of 67 °C and f_{comp} of 30 Hz. (B): WF C_3/C_5 at T_{st} of 60 °C and f_{comp} of 70 Hz. (C): WF C_4 at T_{st} of 89 °C and f_{comp} of 70 Hz. (D): WF C3/C5 at T_{st} of 91 °C and f_{comp} of 70 Hz.

Fig. 2 presents four T-$\dot{H}$-diagrams, based on the experimental results. Each row compares a pure working fluid with the mixture at similar storage temperatures T_{st}; the upper row at $T_{\mathrm{st}} \approx 60$ °C and the lower row at $T_{\mathrm{st}} \approx 90$ °C. T_{st} is the inlet temperature of the storage fluid into the hot storage tank. All operation points are measured at a compressor frequency of $f_{\mathrm{comp}} = 70$ Hz, except for propane with 30 Hz. The plotted WF temperatures in the two-phase region are evaluated as a function of enthalpy and pressure, assuming an isobaric heat exchanger using REFPROP [22]. For pure working fluids, the temperature differences between WF and SFH at the condenser outlet are large. At both storage temperature levels (rows), the mixture's temperature glide improves condenser temperature matching between the WF and SFH. Temperature glides of 26-28 K were observed in the condenser. Deep subcooling was obtained, with the liquid temperature at the subcooler outlet approaching near-ambient conditions (i.e., the SFH inlet temperature). Subcooling up to 59 K was observed at operating points with a high bubble-point temperature $T'(p_3)$ (Fig. 2 (C)).

The non-linearity of the temperature glide can require a higher upper pressure level of the working fluid to reach the desired storage inlet temperature. This can be seen in Fig. 2 (B): For the mixture at T_{st} of 60 °C, a minimum approach temperature of 1.3 K is found near a vapor quality of ca. 0.5, due to the lowered bubble point temperature and a similar steepness of temperature glide and SFH temperature profile. This shifts the WF pressure upwards. Higher WF pressures, however, require a larger compressor power. By correctly matching storage temperatures to the fluid mixture, this effect can be mitigated as shown in Fig. 2 (D): The same mixture at a higher T_{st} of 90 °C, the pressure level is not increased as the minimum approach temperature is shifted close to a vapor quality of 1. Thus, the non-linear temperature glide does not necessarily lead to increased WF pressures for configurations with a single TES on the hot side. A minor crossing of the temperature profiles is observed in this region, most likely due to temperature measurement uncertainties. According to the 2nd law of thermodynamics, temperature profiles cannot cross. This crossing was observed for several operation conditions including pure working fluids; thus, it cannot be explained merely by imprecise mixture EOS or deviations in the mixture composition. Oil could reduce the dew point temperature, but, no considerable amount of oil was detected for the pure WFs, as measured after the sub-cooler.

Because no cold TES is available on the evaporator side to reach temperatures below 0 °C, the tap-water heat source leads to large mean temperature differences that are unfavorable for the WF mixtures. As a result, evaporator exergy destruction exceeds the condenser-side reduction, so we focus on the other components.

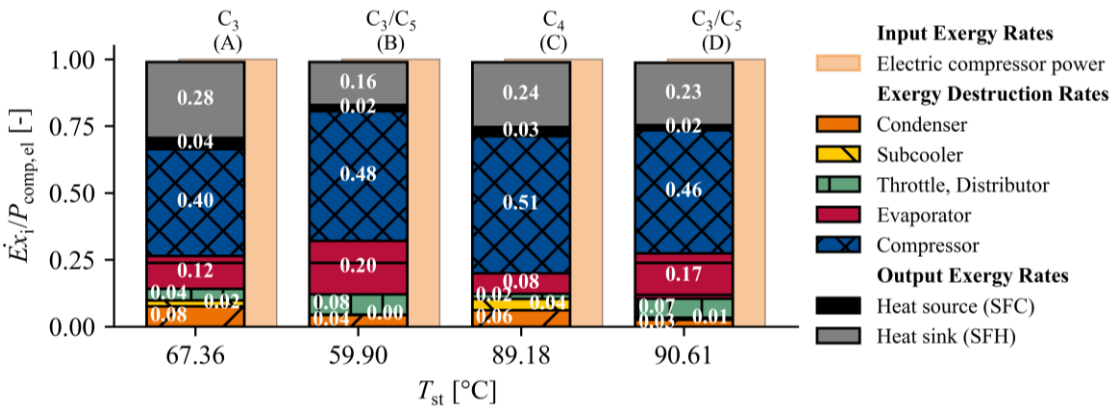

Fig. 3. Exergy input, output and destruction rates normalized by electrical compressor power for the same four working fluids and operation conditions (A-D) as in Fig. 2.

The temperature matching effects can be quantified by analyzing the exergy destruction rates inside the individual components. For that, exergy destruction rates, normalized by the respective compressor power $P_{comp,el}$ of each experiment, are shown in Fig. 3 for the same four operation conditions (A-D) as in Fig. 2. For both pure fluids, ca. 10% of the input exergy is destroyed inside the condenser and subcooler combined. For both WF mixture conditions, these values are reduced to ca. 4%. Comparing the mixture at different T_{st} (conditions B and D), it is observed that an increase in T_{st} leads to reduced exergy destruction rates in the condenser, while the exergy destruction rate in the subcooler increases, both by ca. 1% point. Concluding, an improved exergetic performance is observed for the mixture during heat rejection. These improvements are, however, outweighed by increased exergy destruction in the evaporator and the expansion process (throttle and distributor) for the mixture. The large exergy destruction inside the evaporator could easily be reduced for mixtures, if a heat source with larger temperature changes was used, as planned for future work. By far the largest share of exergy destruction occurs in the compressor. The mixture performs worse than pure propane (C_3) at low T_{st}, but at T_{st} = 90 °C it outperforms pure butane (C_4). These results should be interpreted in light of the compressor being designed for C_3; moreover, the C_3 experiments were conducted at lower rotational speeds at which the compressor exhibits higher efficiency, which limits the fairness of a direct comparison.

3.2. Compressor efficiency

The compressor performance is analyzed in Fig. 4, showing the global compressor efficiency for all investigated operation conditions. The mixture C_3/C_5 reaches global efficiencies between 47 and 57%. Comparing C_4 and C_3/C_5 at the same T_{st} and f_{comp}, the global efficiencies of the mixture are throughout larger. This goes hand in hand with the already discussed lower relative exergy destruction rate in the compressor observed for the mixture. For both WFs, C_3/C_5 and C_4, the following trends are observable: Firstly, increasing

f_{comp} decreases the compressor efficiency. Secondly, the compressor efficiency increases with T_{st}, indicating that the maximum efficiency is presumably at even higher T_{st}. Both trends are not observed for C_3, probably

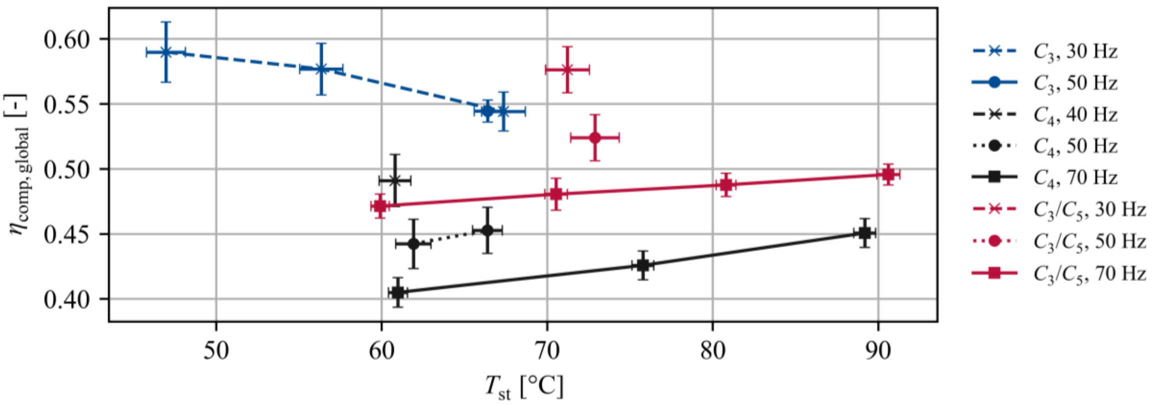

Fig. 4: Measured global compressor efficiency $\eta_{\mathrm{comp,global}}$ for all working fluids (C_3, C_4, C_3/C_5) at various compressor frequencies f_{comp} (in Hz) as a function of storage inlet temperature T_{st}.

the investigated conditions are beyond the optimum: The compressor efficiencies decline with increasing T_{st}. Not enough data points were collected to draw a clear conclusion on the frequency dependence of propane.

The isentropic and volumetric compressor efficiencies of a semi-empirical compressor model (described in section 2.5) are compared with experimental results next, to assess the model and experiment. Fig. 5 shows the simulated isentropic and volumetric efficiencies versus the measured values. Only the measurements for 70 Hz compressor frequency are analyzed in this section, as frequency variation is beyond the scope of the compressor model. The shape of the points indicates the fluid; gray points were simulated with corrected compressor outlet temperatures $T_{2,\mathrm{cor}}$, as described in section 2.2. The filled point was used to calibrate the model. Additionally, ±2% deviation lines are included. The isentropic efficiency varies between 54 and 69%; the volumetric efficiencies vary between 43 and 52%, underlining the importance of using detailed machine models; assuming constant efficiencies would lead to large errors. Both plots prove a generally good agreement between measurement data and simulation, except for the volumetric efficiency of C_4 with up to 15% deviation. This shows the capability of the semi-empirical model to extrapolate to other fluids with only a single experimental point for fitting.

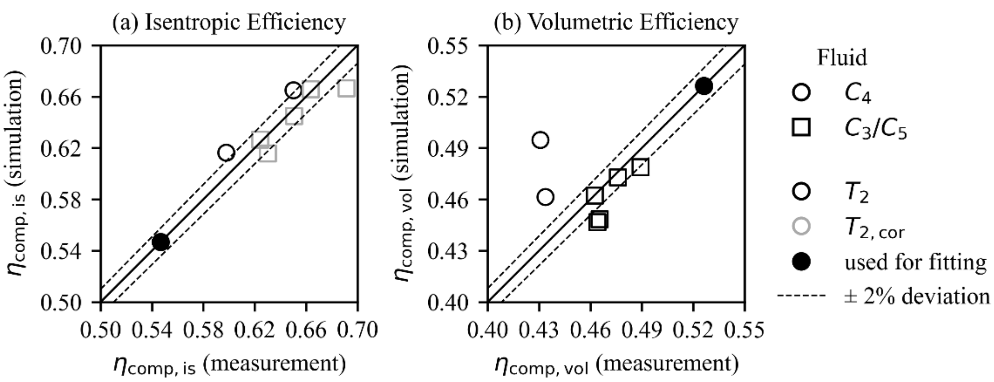

Fig. 5. Comparison of measurements and simulation results for $\eta_{\mathrm{comp,is}}$ and $\eta_{\mathrm{comp,vol}}$. Shapes indicate the fluid (mixture), as given in the legend. The filled point was used for fitting the model. Gray symbols indicate the usage of corrected compressor outlet temperatures.

Fig. 6 shows the pressure ratio dependence of the isentropic and volumetric efficiencies for C_4 and C_3/C_5 at 70 Hz. Both, measurements and simulation results are presented. The inlet state for butane varies by up to 30 kPa and 5 K, which should be kept in mind when interpreting the influence of the pressure ratio. The fluctuations are however considered in the simulation. The inlet state for C_3/C_5 is almost constant and allows a direct interpretation of the pressure ratio results. As expected, the isentropic efficiency depends strongly on the pressure ratio. The predicted difference between both fluids is small with less than 1 percentage point difference, the experiments show a similar tendency within the uncertainties. The volumetric efficiency on the other hand depends stronger on the working fluid. As discussed earlier, the C_4 measurements deviate significantly from the simulation data, exceeding measurement uncertainty. As fluctuations in the inlet state are considered during calculation, the reason for the mismatch could not be finally clarified and could also indicate deviations in the mass flow measurements, this will be analyzed further in future work.

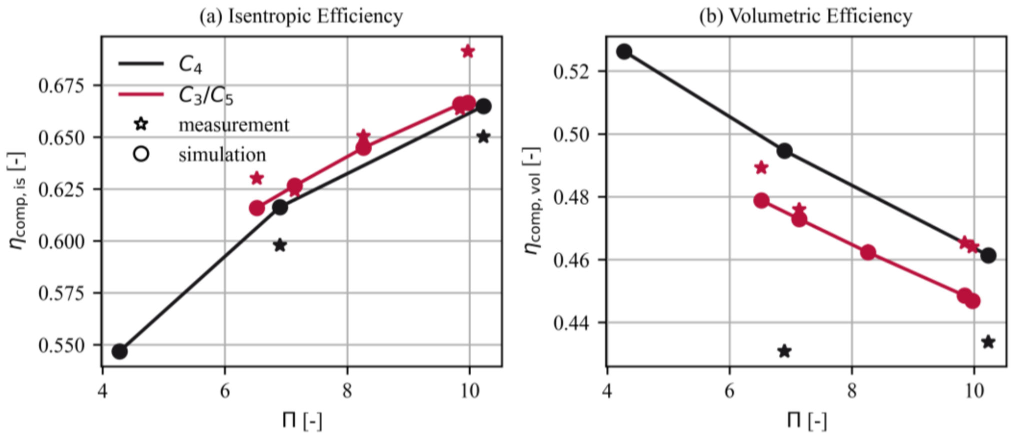

Fig. 6. Isentropic and volumetric compressor efficiency for 70 Hz measurements (working fluids C_4 and C_3/C_5). Simulation date from semi-empirical compressor model, fitted on a measurement point using butane (marked with [fitting] in Table 4). Inlet state of butane varies by up to 30 kPa and 5 K.

3.3. Overall efficiency

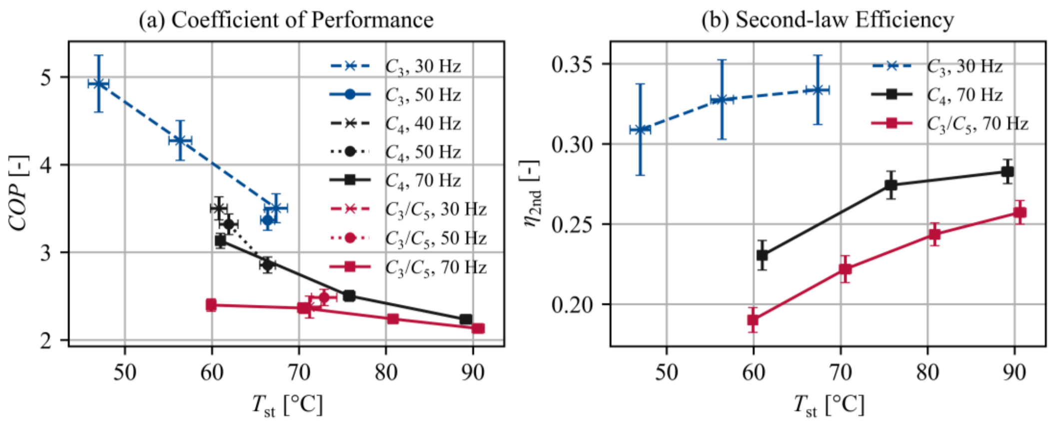

Fig. 7:. Measured *COP* (a) and second-law efficiency η_{2nd} (b) as a function of storage inlet temperature T_{st} for all working fluids (C_3, C_4, C_3/C_5) at various compressor frequencies f_{comp} (in Hz).

After investigating the individual components, the aggregated cycle performance is addressed in this chapter. It should be kept in mind that the actual evaporator temperature levels are not optimal, because no low temperature storage for temperatures below 0 °C is included. Fig. 7 (a) shows *COP*s for all working fluids at varying storage inlet temperature T_{st} and compressor frequency f_{comp}. At lower T_{st} around 60 °C, the *COP*s for C_4 are higher than for C_3/C_5. With increasing T_{st} the difference between C_4 and the mixture decreases. At 90 °C both *COP*s are similar, because the avoidable irreversibilities in the evaporator are now compensated by the reduced ones in the condenser and compressor. The influence of compressor frequency on *COP* is within the uncertainty range.

However, not only for CB applications, the second-law efficiency η_{2nd} is more instructive when temperature levels are varied, which influence the limiting COP_{max}. The second-law efficiency η_{2nd} is shown in Fig. 7 (b). It increases for all working fluids with increasing T_{st}. C_4 shows higher second-law efficiencies than the mixture C_3/C_5 for all T_{st}. The difference decreases slightly with increasing T_{st}, however the change is within the uncertainty range. At T_{st} of 90 °C second-law efficiencies of 25.7 and 28.3% are observed for the two working fluids. These findings show good agreement with the results from the exergy analysis and are now extended to the entire range of T_{st}. It can be concluded that without a heat source with larger temperature change the mixture does not improve η_{2nd} compared to the pure working fluid C_4. Thus, the integration of a low-temperature TES coupled to the evaporator will be investigated in the future. This configuration could improve the performance of heat pumps using working fluid mixtures. By adjusting the mass flow rate of the storage fluid, its outlet temperature can be brought close to the evaporator inlet working fluid temperature, enhancing temperature profile matching and the second-law efficiency.

4. Conclusions

A laboratory-scale heat pump coupled to a single thermal energy storage as heat sink for Carnot battery applications was investigated experimentally. Storage temperatures always started at ambient conditions and reached values up to 90 °C. The aim was especially to investigate how the thermodynamic performance of the compressor and the condenser are affected when a high-glide mixture of C_3/C_5 is used compared to two pure working fluids – propane and butane. The compressor performance was compared to a semi-empirical compressor model from literature.

- The working fluid mixture C_3/C_5 successfully reduced exergy destruction inside the condenser and subcooler due to improved temperature profile matching. Simultaneously, exergy losses in the throttling and the – non-optimized – evaporator increased.
- The global compressor efficiency for the mixture is throughout higher than for butane, which is the pure fluid, suitable for high storage temperatures.
- The overall exergetic efficiency of the mixture was lower than the pure fluids, because the evaporator temperature levels were not optimized here. This highlights the need for a heat source with large temperature change to reach the full potential of high-glide mixtures.
- The compressor model predicted the measured isentropic efficiencies well, indicating its suitability for fluid-dependent heat pump simulations. The model-predicted volumetric efficiencies agree less good with the experimental data, which may be an experimental problem, as will be analyzed in future work.

In the future an expansion of the experimental set-up is planned, adding a further sensible storage coupled to the evaporator for temperatures down to -25 °C and expanding it to a Carnot battery. Also, different working fluid mixtures and compositions shall be investigated, because experimental work on such systems is scarce and reveals important coupling effects in thermodynamic cycles.

Acknowledgements

The authors gratefully acknowledge the financial support by the Deutsche Forschungsgemeinschaft (DFG), grant number 525971077, within the framework of the DFG priority programme SPP 2403 ‘Carnot-Batteries: Inverse Design from Markets to Molecules’. We also gratefully acknowledge the following companies for providing components: Bitzer (compressor and FI), Frigomec (liquid receiver), and Sanhua (expansion valve).

Declaration of AI-assisted technologies

During the preparation of this manuscript, the authors used ChatGPT (OpenAI) and DeepL to assist with code generation and language editing. The authors reviewed and edited all AI-assisted output and take full responsibility for the content of the publication.

Data availability

The experimental data are available on Zenodo at https://doi.org/10.5281/zenodo.18712882.

References

[1] J. Mutke, L.S. Plaga, V. Bertsch, Influence of bioenergy and transmission expansion on electrical energy storage requirements in a gradually decarbonized European power system, Journal of Cleaner Production 419 (2023) 138133, https://doi.org/10.1016/j.jclepro.2023.138133.

[2] O. Dumont, G.F. Frate, A. Pillai, S. Lecompte, M. de paepe, V. Lemort, Carnot battery technology: A state-of-the-art review, Journal of Energy Storage 32 (2020) 101756,

https://doi.org/10.1016/j.est.2020.101756.

[3] A. Koen, P. Farres-Antunez, J. Macnaghten, A. White, A low-temperature glide cycle for pumped thermal energy storage, Journal of Energy Storage 42 (2021) 103038, https://doi.org/10.1016/j.est.2021.103038.

[4] A. Bernehed, ZeoPTES: Zeotropic Pumped Thermal Energy Storage with an Ammonia–Water Mixture as Working Fluid, Energy Technol. 9 (2021), https://doi.org/10.1002/ente.202100470.

[5] A. Welp, B. Atakan, Modelling strategy for efficiency optimization of Carnot batteries with sensible storages and zeotropic mixtures, 38th International Conference on Efficiency, Cost, Optimization, Simulation and Environmental Impact of Energy Systems (ECOS) (2025) Paper ID: 7509.

[6] M. Weitzer, M. Moderegger, L. Metzner, S. Kolb, J. Karl, Reversible heat pump - Organic Rankine Cycle systems with zeotropic fluid mixtures for enhanced performance - Experimental and simulative results from a pilot plant, 20th International Refrigeration and Air Conditioning Conference at Purdue (2024), https://docs.lib.purdue.edu/iracc/2614.

[7] M. Weitzer, S. Reiß, D. Steger, S. Kolb, J. Karl, Experimental characterization of a reversible heat pump – Organic Rankine cycle pilot plant as a thermally integrated Carnot battery, Applied Thermal Engineering 260 (2025) 124872, https://doi.org/10.1016/j.applthermaleng.2024.124872.

[8] A. Thess, Thermodynamic efficiency of pumped heat electricity storage, Physical review letters 111 (2013) 110602, https://doi.org/10.1103/PhysRevLett.111.110602.

[9] B. Atakan, Thermodynamic analysis of Carnot Batteries: Storage temperatures, sensitivities, and optimal parameters (2024), https://dx.doi.org/10.2139/ssrn.4775278.

[10] L.P. Brendel, S.N. Bernal, P. Widmaier, D. Roskosch, C. Arpagaus, A. Bardow, S.S. Bertsch, High-glide refrigerant blends in high-temperature heat pumps: Part 1 – Coefficient of performance, International Journal of Refrigeration 165 (2024) 84–96, https://doi.org/10.1016/j.ijrefrig.2024.05.005.

[11] J. Quenel, M. Anders, B. Atakan, Propane-isobutane mixtures in heat pumps with higher temperature lift: An experimental investigation, Thermal Science and Engineering Progress 42 (2023) 101907, https://doi.org/10.1016/j.tsep.2023.101907.

[12] V. Venzik, D. Roskosch, B. Atakan, Propene/isobutane mixtures in heat pumps: An experimental investigation, International Journal of Refrigeration 76 (2017) 84–96, https://doi.org/10.1016/j.ijrefrig.2017.01.027.

[13] L.P.M. Brendel, S.N. Bernal, C. Arpagaus, D. Roskosch, A. Bardow, S.S. Bertsch, Experimental Performance Comparison of High-Glide Hydrocarbon and Synthetic Refrigerant Mixtures in a High-Temperature Heat Pump, Energies 17 (2024) 1981, https://doi.org/10.3390/en17081981.

[14] H. Mehmood, S. Teng, H. Xi, Thermo-economic parametric evaluation of different configurations of pumped thermal energy storage system using zeotropic fluids, Journal of Energy Storage 131 (2025) 117517, https://doi.org/10.1016/j.est.2025.117517.

[15] M. Muneeshwaran, H.J. Kim, M. Tayyab, W. Li, K. Nawaz, C.-M. Yang, Flow maldistribution in plate heat exchangers – Impact, analysis, and solutions, Renewable and Sustainable Energy Reviews 207 (2025) 114905, https://doi.org/10.1016/j.rser.2024.114905.

[16] Bitzer SE, Technische Information KT-500-10 BITZER Kältemaschinenöle für Hubkolbenverdichter, 2025, https://www.bitzer.de/shared_media/html/kt-500/de-DE/index.html?P=/html/kt-500/de-DE&N=index.html#265616139265617931, accessed 29 October 2025.

[17] Bitzer SE, OPERATING INSTRUCTIONS KB-100-2, 2024, https://www.bitzer.de/shared_media/documentation/kb-100-2.pdf?P=/doc/&N=kb-100-2.pdf, accessed 29 October 2025.

[18] J. Heywood, Internal Combustion Engine Fundamentals, McGraw-Hill, NewYork, 1988.

[19] D. Roskosch, V. Venzik, B. Atakan, Thermodynamic model for reciprocating compressors with the focus on fluid dependent efficiencies, International Journal of Refrigeration 84 (2017) 104–116, https://doi.org/10.1016/j.ijrefrig.2017.08.011.

[20] L.P. Brendel, S.N. Bernal, C. Hemprich, A.J. Rowane, I.H. Bell, D. Roskosch, C. Arpagaus, A. Bardow, S.S. Bertsch, High-glide refrigerant blends in high-temperature heat pumps: Part 2 – Inline composition determination for binary mixtures, International Journal of Refrigeration 165 (2024) 45–57, https://doi.org/10.1016/j.ijrefrig.2024.05.012.

[21] S.S. Wujek, P.S. Hrnjak, Using Density to Calculate the Oil Circulation Ratio of a PAG Oil in R134a, SAE International Journal of Materials and Manufacturing 1 (2009) pp. 362-368, https://www.jstor.org/stable/10.2307/26282665.

[22] E.W. Lemmon, I.H. Bell, M.L. Huber, M. McLinden, NIST Standard Reference Database 23: Reference Fluid Thermodynamic and Transport Properties-REFPROP, Version 10.0, National Institute of Standards and Technology, Standard Reference Data Program, Gaithersburg, 2018.

[23] J. Herman, W. Usher, SALib: An open-source Python library for Sensitivity Analysis, JOSS 2 (2017) 97, https://joss.theoj.org/papers/10.21105/joss.00097.